INTERNATIONAL JOURNAL FOR NUMERICAL METHODS IN ENGINEERING
Int. J. Numer. Meth. Engng 2007; **71**:837–855
Published online 5 February 2007 in Wiley InterScience (www.interscience.wiley.com). DOI: 10.1002/nme.2000

A dual BIE approach for large-scale modelling of 3-D electrostatic problems with the fast multipole boundary element method

Y. J. Liu*,† and L. Shen

Department of Mechanical, Industrial and Nuclear Engineering, University of Cincinnati, P.O. Box 210072, Cincinnati, OH 45221-0072, U.S.A.

SUMMARY

A dual boundary integral equation (BIE) formulation is presented for the analysis of general 3-D electrostatic problems, especially those involving thin structures. This dual BIE formulation uses a linear combination of the conventional BIE and hypersingular BIE on the entire boundary of a problem domain. Similar to crack problems in elasticity, the conventional BIE degenerates when the field outside a thin body is investigated, such as the electrostatic field around a thin conducting plate. The dual BIE formulation, however, does not degenerate in such cases. Most importantly, the dual BIE is found to have better conditioning for the equations using the boundary element method (BEM) compared with the conventional BIE, even for domains with regular shapes. Thus the dual BIE is well suited for implementation with the fast multipole BEM. The fast multipole BEM for the dual BIE formulation is developed based on an adaptive fast multiple approach for the conventional BIE. Several examples are studied with the fast multipole BEM code, including finite and infinite domain problems, bulky and thin plate structures, and simplified comb-drive models having more than 440 thin beams with the total number of equations above 1.45 million and solved on a PC. The numerical results clearly demonstrate that the dual BIE is very effective in solving general 3-D electrostatic problems, as well as special cases involving thin perfect conducting structures, and that the adaptive fast multipole BEM with the dual BIE formulation is very efficient and promising in solving large-scale electrostatic problems. Copyright © 2007 John Wiley & Sons, Ltd.

Received 7 June 2006; Revised 21 December 2006; Accepted 22 December 2006

KEY WORDS: boundary element method; fast multipole method; 3-D electrostatic problems

*Correspondence to: Y. J. Liu, Department of Mechanical, Industrial and Nuclear Engineering, University of Cincinnati, P.O. Box 210072, Cincinnati, OH 45221-0072, U.S.A.
†E-mail: Yijun.Liu@uc.edu

Contract/grant sponsor: U.S. National Science Foundation; contract/grant number: CMS-0508232

1. INTRODUCTION

The boundary element method (BEM) [1–5] is well suited for the analysis of electrostatic fields as existing in micro-electro-mechanical systems (MEMS), because of the advantages of the BEM in handling complicated geometries and infinite domains. Some of the early work using the BEM for modelling electrostatic MEMS problems can be found in References [6–8]. Some recent work can be found in [9–12] for solving various electrostatic problems, including those involving thin conducting beams and thin plates [9, 10] which are similar to crack problems in elasticity. Most recently, dual boundary integral equation (BIE) approaches using both the conventional BIE and hypersingular BIE for modelling 2-D electrostatic MEMS problems have been proposed by Liu [13]. These dual BIE approaches are found to be very efficient in analysing complicated MEMS problems with very thin structures and also show better conditioning for the systems of the BEM equations. In the literature, a dual BIE approach has also been applied in [12] to MEMS problems for estimating the errors in the BEM solutions and for directly computing the tangential electric field. In the context of Stokes flow, a dual BIE formulation has been proposed in [14–16] for evaluating damping forces in MEMS. To the authors' best knowledge, the suitability of the dual BIEs for modelling 3-D electrostatic problems with thin structures and their implementations with the fast multipole BEM have not been reported in the literature.

Analysis of MEMS problems often requires large models that can accurately predict the rapidly changing fields surrounding complicated structures. The conventional BEM approach requires $O(N^3)$ operations to solve the BEM system using direct solvers (with N being the number of equations) or $O(N^2)$ operations using iterative solvers. Thus the conventional BEM is often found inefficient in solving large-scale problems with the number of equations above a few thousands. The fast multipole method (FMM) [17–19] and other fast methods can be used to accelerate the solutions of the BEM by several folds, promising to reduce the CPU time and memory usage in the fast multipole-accelerated BEM to $O(N)$. A comprehensive review of the fast multipole-accelerated BEM can be found in Reference [20] and a recent tutorial paper can be found in [21]. Some of the applications of the fast multipole and other related fast BEM approaches for modelling general electrostatic or MEMS problems can be found in [14, 15, 22–25] using the FMM and in [26, 27] using the precorrected-FFT method.

In this paper, a dual BIE formulation is investigated for the analysis of general 3-D electrostatic problems that can involve thin-beam and thin-plate structures as found in MEMS. This dual BIE formulation (to be referred to as CHBIE) uses a linear combination of the conventional BIE (CBIE) and the hypersingular BIE (HBIE) on all surfaces of the problem domain that can be finite or infinite. This dual BIE approach has been shown to be very effective in solving crack-like problems [28, 29], which in the current context, can involve the electrostatic fields surrounding thin beams or thin plates of arbitrarily small thickness. As in the 2-D case [13], this dual BIE approach for 3-D electrostatic problems is found to be very stable for extremely small thickness of thin plate structures (with the thickness-to-length ratio less than 10^{-6}). It also provides better conditioning for the BEM systems of equations for other problems with bulky 3-D shapes, as compared with the conventional BIE. Thus, this dual BIE approach is well suited for implementation with the FMM. The recently developed adaptive fast multipole BEM for general 3-D potential problems based on the CBIE [30] is extended to this dual BIE formulation for general electrostatic problems to accelerate the BEM solutions. Several numerical examples are studied and the effectiveness and accuracy of the dual BIE accelerated by the fast multipole BEM are clearly demonstrated by the numerical results.

DOI: 10.1002/nme

This paper is organized as follows: In Section 2, the BIE formulations for 3-D electrostatic problems are reviewed. In Section 3, the fast multipole BEM for the BIEs is summarized. In Section 4, numerical examples are presented to demonstrate the effectiveness of the dual BIE formulation and the efficiencies of the fast multipole BEM for large-scale problems. The paper concludes with some discussions in Section 5.

2. THE BIE FORMULATIONS

Consider a 3-D domain V (which can be infinite, as shown in Figure 1, or finite). The electric potential ϕ in V satisfies the Laplace equation and can be given by the following representation integral:

$$\phi(\mathbf{x}) = \int_S [G(\mathbf{x}, \mathbf{y})q(\mathbf{y}) - F(\mathbf{x}, \mathbf{y})\phi(\mathbf{y})]\, \mathrm{d}S(\mathbf{y}) + C \quad \forall \mathbf{x} \in V \tag{1}$$

where S is the boundary, $q = \partial\phi/\partial n$, and n the outward normal (Figure 1). $G(\mathbf{x}, \mathbf{y})$ is the 3-D Green's function given by

$$G(\mathbf{x}, \mathbf{y}) = \frac{1}{4\pi r} \quad \text{and} \quad F(\mathbf{x}, \mathbf{y}) = \frac{\partial G(\mathbf{x}, \mathbf{y})}{\partial n(\mathbf{y})} \tag{2}$$

with $r = |\mathbf{x} - \mathbf{y}|$. C is a constant representing the potential at infinity (which vanishes for finite domain problems). In electrostatics, the charge density σ is defined by

$$\sigma(\mathbf{y}) \equiv \varepsilon q(\mathbf{y}) \tag{3}$$

where ε is the dielectric constant.

Letting the source point $\mathbf{x}$ approach boundary S in Equation (1), one obtains the *conventional BIE* (CBIE) for potential problems:

$$\frac{1}{2}\phi(\mathbf{x}) = \int_S [G(\mathbf{x}, \mathbf{y})q(\mathbf{y}) - F(\mathbf{x}, \mathbf{y})\phi(\mathbf{y})]\, \mathrm{d}S(\mathbf{y}) + C \quad \forall \mathbf{x} \in S \tag{4}$$

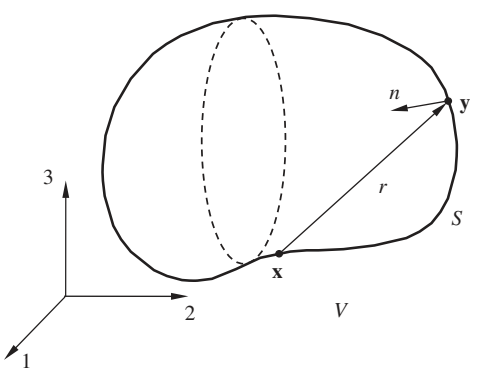

Figure 1. An infinite domain V outside surface S.

DOI: 10.1002/nme

for boundary S which is smooth near the source point $\mathbf{x}$, where the second integral with the singular kernel F on the right-hand side is a Cauchy-principal value (CPV) type of integral.

Taking the derivative of Equation (1) with $\mathbf{x} \in V$ and then letting $\mathbf{x}$ go to the boundary, one obtains the following *hypersingular BIE* (HBIE):

$$\frac{1}{2}q(\mathbf{x}) = \int_S [K(\mathbf{x}, \mathbf{y})q(\mathbf{y}) - H(\mathbf{x}, \mathbf{y})\phi(\mathbf{y})]\, \mathrm{d}S(\mathbf{y}) \quad \forall \mathbf{x} \in S \tag{5}$$

in which the two new kernels are given by

$$K(\mathbf{x}, \mathbf{y}) = \frac{\partial G(\mathbf{x}, \mathbf{y})}{\partial n(\mathbf{x})} \quad \text{and} \quad H(\mathbf{x}, \mathbf{y}) = \frac{\partial F(\mathbf{x}, \mathbf{y})}{\partial n(\mathbf{x})} = \frac{\partial^2 G(\mathbf{x}, \mathbf{y})}{\partial n(\mathbf{x}) \partial n(\mathbf{y})} \tag{6}$$

In Equation (5), the first integral with the K kernel is a singular (CPV) integral, while the second integral with the H kernel is a hypersingular integral in the sense of Hadamard-finite part (HFP) (see, e.g. [31–33]).

Note that for perfect conductors, electric potential $\phi =$ constant on each of the conductors, and the second integral, with F kernel in Equation (4) or with H kernel in Equation (5), vanishes due to the properties of the kernels (see, e.g. References [13, 34]), which leads to two reduced BIEs from Equations (4) and (5). These reduced BIEs contain weakly-singular kernel G only for Equation (4) and strongly-singular kernel K only for BIE (5), which can simplify significantly the BEM implementation for models of perfect conductors, as used in Reference [13] for 2-D electrostatic problems. In this study, however, CBIE (4) and HBIE (5) in their original forms will be used with the BEM so that general 3-D electrostatic problems can be tackled by the developed BEM approach, including modelling perfect conductors, semi-conductors and other general 3-D potential problems.

It is also interesting to note that HBIE (5) cannot be applied *alone* to solve general potential problems in multiple-connected domains, such as the analysis of a block with one or more voids, when q is specified on these voids. The solutions of ϕ on the surfaces of these voids will be non-unique since adding a constant ϕ_0 to the solution ϕ on a void surface S_H will not change the hypersingular BIE (5), that is,

$$\int_{S_H} H(\mathbf{x}, \mathbf{y})[\phi(\mathbf{y}) + \phi_0]\, \mathrm{d}S(\mathbf{y}) = \int_{S_H} H(\mathbf{x}, \mathbf{y})\phi(\mathbf{y})\, \mathrm{d}S(\mathbf{y}) \quad \forall \mathbf{x} \in S$$

because

$$\int_{S_H} H(\mathbf{x}, \mathbf{y})\, \mathrm{d}S(\mathbf{y}) = 0 \quad \forall \mathbf{x} \in V \cup S$$

due to the properties of the hypersingular kernel H [34]. This interesting issue with the HBIE has been addressed in References [35–37].

It is well known that the CBIE (4) will degenerate for crack-like problems, such as in solving the electric fields outside a thin beam or thin plate, similar to the crack problems in elasticity (see, e.g. References [2, 38, 39]). To remedy this situation, the dual BIE (or composite BIE) approaches combining the CBIE and HBIE have been proven to be very effective for crack problems [28, 29]. The advantages of using the dual BIE approaches are that they are valid for both open crack and true crack cases, without the need to switch the BIE formulations, and the original boundary variables can be solved directly. Because of the similarities mentioned above, the dual BIE approaches

DOI: 10.1002/nme

should be equally effective in solving electrostatic problems in domains surrounding thin beams or thin plates.

In Reference [13], two dual BIE formulations are tested for solving 2-D electrostatic fields surrounding thin beam perfect conductors. The first dual BIE approach uses CBIE on one surface of a thin beam and the HBIE on the other surface. The second dual BIE approach uses a linear combination of the CBIE and HBIE on all surfaces of the beams. Both dual BIE approaches are found to be very effective in solving thin beam problems [13]. However, the second dual BIE approach, using a linear combination of the CBIE and HBIE, offers better conditioning for the system of equations in the BEM and thus is more suitable for the fast multipole implementation.

In this paper, a linear combination of CBIE (4) and HBIE (5) in the form,

$$(\text{CBIE}) + \beta \cdot (\text{HBIE}) \tag{7}$$

with β being a constant, is applied for solving general 3-D electrostatic problems, especially problems with thin beams or thin plates. This dual BIE, also termed CHBIE, does not degenerate for domains containing thin beams or thin plates. At the same time, this dual BIE offers better conditioning for the BEM systems of equations, even for regular domains of bulky shapes, which will facilitate faster convergence when using the fast multipole BEM.

The selection of the coupling constant β is crucial for the performance of the dual BIE. There is so far no unified formula regarding the selection of the values of β in the electrostatic BIE. The selection is case dependent. A general rule is that the constant β should be selected such that HBIE does *not* dominate in the dual BIE formulation (7) (In fact, for a perfect conductor, HBIE is a homogeneous and singular equation, and thus cannot be solved alone [13–15]). It is also noted that β should have the unit of length, so that the two terms in Equation (7) will have a consistent unit. In the study of 2-D MEMS problems with thin beams [13], the choice of $\beta = h_0 - h$ has been found to be sufficient, with h_0 being a reference, initial thickness and h the current thickness of the beam. This means that the influence of the HBIE in Equation (7) gradually increases as the thickness of the beams decreases. For exterior acoustic problems, Equation (7) is the Burton–Miller formulation that is very effective in overcoming the fictitious eigenfrequency difficulties (see, e.g. [40, 41]), where β is an imaginary number for problems with real wave numbers and a real number for those with imaginary wave numbers.

Both the conventional BEM and fast multipole BEM codes based on the above BIE formulations (CBIE (4), HBIE (5), and CHBIE (7)) have been developed in this study. Constant elements (flat triangles) are used, for which all the integrals (with G, F, K, and H kernels) in BIEs (4) and (5) can be integrated analytically, whether they are non-singular, nearly-singular, strongly singular or hypersingular. Thus, the codes can handle very thin plates or shells with very small but finite thickness or small gaps in models of electrostatic problems, without any difficulties regarding the singular and hypersingular integrals.

3. THE FAST MULTIPOLE METHOD (FMM)

The new adaptive FMM developed in [30] for 3-D potential problems with the CBIE (4) is extended to solve the CHBIE (7). The main idea of the FMM is to translate the node-to-node (or element-to-element) interactions to cell-to-cell interactions using various expansions and translations. The FMM can be used in the iterative equation solvers (such as GMRES), in which matrix–vector multiplications are calculated using fast multipole expansions. Adopting the FMM in the iterative

DOI: 10.1002/nme

solvers for the systems of the BEM equations, both the solution time and memory requirement for solving a problem can be reduced to $O(N)$, with N being the total number of unknowns.

The fast multipole BEM for 3-D potential problems has been well documented (see, e.g. References [19, 20, 30]). For completeness, the main results for CBIE (4) are summarized first and then the treatment of the HBIE (5) is discussed.

The kernel G in Equation (2) can be written with a series expansion as

$$G(\mathbf{x}, \mathbf{y}) = \frac{1}{4\pi r} \cong \frac{1}{4\pi} \sum_{n=0}^{p} \sum_{m=-n}^{n} \overline{S_{n,m}}(\mathbf{x}, \mathbf{y}_c) R_{n,m}(\mathbf{y}, \mathbf{y}_c), \quad |\mathbf{x} - \mathbf{y}_c| > |\mathbf{y} - \mathbf{y}_c| \tag{8}$$

where $\mathbf{y}_c$ is the expansion centre, p is the number of expansion terms, and $\overline{(\,)}$ indicates the complex conjugate. The functions $S_{n,m}$ and $R_{n,m}$ are solid harmonic functions (see, e.g. [42]).

The kernel F in Equation (2) can also be expanded as

$$F(\mathbf{x}, \mathbf{y}) = \frac{\partial G(\mathbf{x},\mathbf{y})}{\partial n(\mathbf{y})} \cong \frac{1}{4\pi} \sum_{n=0}^{p} \sum_{m=-n}^{n} \overline{S_{n,m}}(\mathbf{x},\mathbf{y}_c) \frac{\partial R_{n,m}(\mathbf{y},\mathbf{y}_c)}{\partial n(\mathbf{y})}, \quad |\mathbf{x} - \mathbf{y}_c| > |\mathbf{y} - \mathbf{y}_c| \tag{9}$$

Applying expansions in Equations (8) and (9), one can evaluate the integrals in Equation (4) on S_0 (a subset of S) which is away from the source point $\mathbf{x}$ using the following *multipole expansions*:

$$\int_{S_0} G(\mathbf{x},\mathbf{y}) q(\mathbf{y})\, \mathrm{d}S(\mathbf{y}) \cong \frac{1}{4\pi} \sum_{n=0}^{p} \sum_{m=-n}^{n} \overline{S_{n,m}}(\mathbf{x},\mathbf{y}_c) M_{n,m}(\mathbf{y}_c), \quad |\mathbf{x} - \mathbf{y}_c| > |\mathbf{y} - \mathbf{y}_c| \tag{10}$$

$$\int_{S_0} F(\mathbf{x},\mathbf{y}) \phi(\mathbf{y})\, \mathrm{d}S(\mathbf{y}) \cong \frac{1}{4\pi} \sum_{n=0}^{p} \sum_{m=-n}^{n} \overline{S_{n,m}}(\mathbf{x},\mathbf{y}_c) \tilde{M}_{n,m}(\mathbf{y}_c), \quad |\mathbf{x} - \mathbf{y}_c| > |\mathbf{y} - \mathbf{y}_c| \tag{11}$$

where $M_{n,m}$ and $\tilde{M}_{n,m}$ are called *multipole moments* centred at $\mathbf{y}_c$ and given by

$$M_{n,m}(\mathbf{y}_c) = \int_{S_0} R_{n,m}(\mathbf{y},\mathbf{y}_c) q(\mathbf{y})\, \mathrm{d}S(\mathbf{y}) \tag{12}$$

$$\tilde{M}_{n,m}(\mathbf{y}_c) = \int_{S_0} \frac{\partial R_{n,m}(\mathbf{y}, \mathbf{y}_c)}{\partial n(\mathbf{y})} \phi(\mathbf{y})\, \mathrm{d}S(\mathbf{y}) \tag{13}$$

Note that these moments are independent of the source point $\mathbf{x}$ and the integrals in Equations (12) and (13) only need to be evaluated once. Translations from moment to moment (M2M), moment to local (M2L), and local to local (L2L) are needed to translate the moments to a *local expansion* that is used to evaluate the integrals away from the source point. In the new fast multipole approach [42, 43], which is used in [30] and this work, the M2L is replaced by M2X, X2X and X2L translations using exponential expansions. Comparisons of the original and new fast multipole approaches regarding the computing efficiencies for 3-D potential problems can be found in Reference [42].

DOI: 10.1002/nme

For the kernels in the HBIE (5), one has the following two expansions due to relation (6):

$$K(\mathbf{x},\mathbf{y})=\frac{\partial G(\mathbf{x},\mathbf{y})}{\partial n(\mathbf{x})}\cong\frac{1}{4\pi}\sum_{n=0}^{p}\sum_{m=-n}^{n}\frac{\partial\overline{S_{n,m}}(\mathbf{x},\mathbf{y}_c)}{\partial n(\mathbf{x})}R_{n,m}(\mathbf{y},\mathbf{y}_c),\quad |\mathbf{x}-\mathbf{y}_c|>|\mathbf{y}-\mathbf{y}_c| \tag{14}$$

$$H(\mathbf{x},\mathbf{y})=\frac{\partial F(\mathbf{x},\mathbf{y})}{\partial n(\mathbf{x})}\cong\frac{1}{4\pi}\sum_{n=0}^{p}\sum_{m=-n}^{n}\frac{\partial\overline{S_{n,m}}(\mathbf{x},\mathbf{y}_c)}{\partial n(\mathbf{x})}\frac{\partial R_{n,m}(\mathbf{y},\mathbf{y}_c)}{\partial n(\mathbf{y})},\quad |\mathbf{x}-\mathbf{y}_c|>|\mathbf{y}-\mathbf{y}_c| \tag{15}$$

Thus, the multipole expansions for the HBIE (5) can be written as

$$\int_{S_0}K(\mathbf{x},\mathbf{y})q(\mathbf{y})\,\mathrm{d}S(\mathbf{y})\cong\frac{1}{4\pi}\sum_{n=0}^{p}\sum_{m=-n}^{n}\frac{\partial\overline{S_{n,m}}(\mathbf{x},\mathbf{y}_c)}{\partial n(\mathbf{x})}M_{n,m}(\mathbf{y}_c),\quad |\mathbf{x}-\mathbf{y}_c|>|\mathbf{y}-\mathbf{y}_c| \tag{16}$$

$$\int_{S_0}H(\mathbf{x},\mathbf{y})\phi(\mathbf{y})\,\mathrm{d}S(\mathbf{y})\cong\frac{1}{4\pi}\sum_{n=0}^{p}\sum_{m=-n}^{n}\frac{\partial\overline{S_{n,m}}(\mathbf{x},\mathbf{y}_c)}{\partial n(\mathbf{x})}\tilde{M}_{n,m}(\mathbf{y}_c),\quad |\mathbf{x}-\mathbf{y}_c|>|\mathbf{y}-\mathbf{y}_c| \tag{17}$$

where the two moments $M_{n,m}$ and $\tilde{M}_{n,m}$ are the same as given in Equations (12) and (13) for the CBIE. It turns out that all the translations for the HBIE are also identical to those for the CBIE. The only difference with the HBIE is in the local expansions.

The details of the adaptive fast multipole approach used in this study can be found in [30], including the construction of an adaptive tree structure for a given domain. For near-field evaluation of the integrals, analytical integrations are used for all the integrals, which is possible with the constant elements used in this study [44]. Block diagonal preconditioner is employed for the GMRES solver, in which the coefficients on elements in a leaf are used to construct the preconditioner. The inverse of the diagonal block matrices can also be saved in memory or on disk for use in each iteration to speed up the fast multipole computation [30].

4. NUMERICAL EXAMPLES

Several numerical examples are presented to demonstrate the effectiveness and accuracy of the CHBIE formulations for electrostatic analysis of problems with different geometries and the efficiency of the fast multipole BEM for modelling large 3-D electrostatic problems. In all the examples, except for the two-parallel plate model, the coupling constant in CHBIE (7) is $\beta=-1$. (The minus sign is due to the way the HBIE is added in Equation (7).)

4.1. A cube model with linear potential

This is a simple interior problem used to test the accuracy of the developed code. The cube has an edge length $=1$ (Figure 2), and is applied with a linear electric potential $\phi(x,y,z)=x$ on all surfaces. The charge density for this problem should be 1 on the surface at $x=0.5$, and -1 on the surface at $x=-0.5$, assuming the dielectric constant $\varepsilon=1$. For the fast multipole BEM, 15 terms are used in all the expansions and the tolerance for convergence is set to 10^{-6}.

Table I shows the results with the conventional BEM and fast multipole BEM, and using the CBIE, HBIE, and CHBIE, for BEM meshes with increasing numbers of elements. One can conclude from these results that the HBIE and CHBIE are equally accurate as the CBIE, so is the

DOI: 10.1002/nme

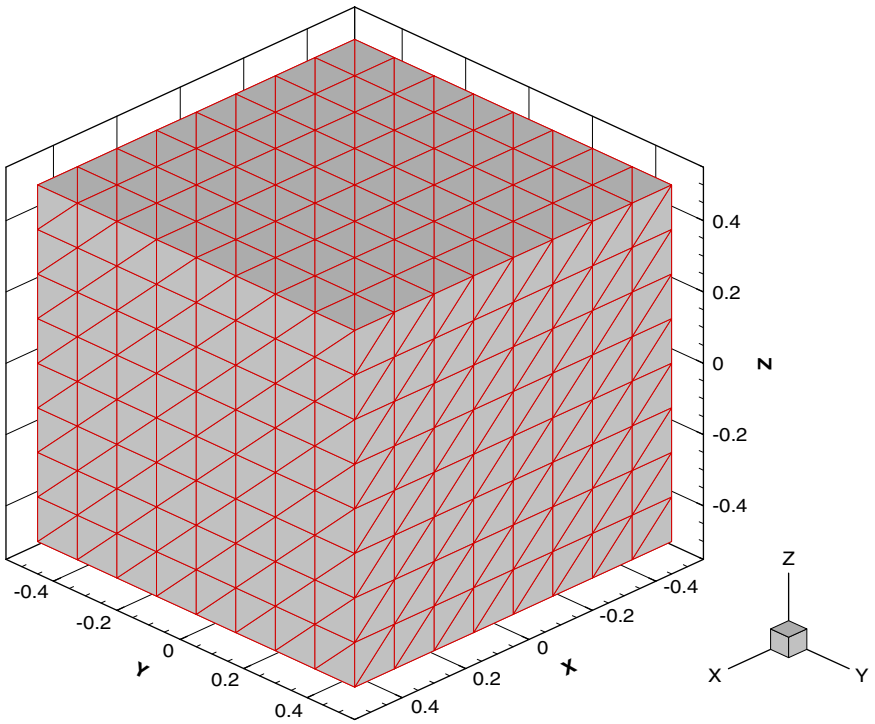

Figure 2. A cube meshed with 768 elements and with linear potential in the x-direction.

Table I. Results for the cube with a linear potential in the x-direction.

Model		Charge density at (0.5, 0, 0)					
		Conventional BEM			Fast multipole BEM		
Elem/edge	DOFs	CBIE	HBIE	CHBIE	CBIE	HBIE	CHBIE
2	48	1.08953	1.07225	1.06800	1.08955	1.07278	1.06843
4	192	0.99124	1.00624	0.99754	0.99124	1.00624	0.99754
8	768	0.99825	1.00438	0.99894	0.99825	1.00438	0.99894
12	1728	0.99908	1.00327	0.99934	0.99908	1.00327	0.99934
16	3072	0.99942	1.00260	0.99953	0.99943	1.00260	0.99953
20	4800	0.99959	1.00216	0.99963	0.99962	1.00218	0.99965
24	6912	0.99969	1.00185	0.99970	0.99969	1.00184	0.99969
28	9408	—	—	—	0.99976	1.00161	0.99975
32	12 288	—	—	—	0.99981	1.00143	0.99979
Exact value		1.00000					

DOI: 10.1002/nme

fast multipole BEM as the conventional BEM. Note that constant triangular elements are used in this study. If linear or quadratic elements were applied, a few elements should have been efficient for obtaining results of a similar accuracy, due to the specified linear field.

4.2. A single conducting sphere model

This is a simple exterior problem used to test the accuracy of the codes for models with curved geometries. The conducting sphere (Figure 3) has a radius $a = 1$ and a constant electric potential $\phi_0 = 1$ is applied on its surface. The analytical solution of the electric field outside the sphere is $\phi = (a/r)\phi_0$ with r being the distance from the centre of the sphere, which gives a charge density on the surface equal to 1 for this case, assuming the dielectric constant $\varepsilon = 1$ and the potential at infinity $C = 0$. For the fast multipole BEM, elements per leaf are set to 100, number of terms in the expansions to 10, and the tolerance for convergence to 10^{-6}.

Table II gives the results of the charge density at the point $(1, 0, 0)$ on the surface of the sphere. For this problem, the HBIE is a homogeneous equation and cannot be solved alone. The CHBIE is slightly less accurate than the CBIE, probably due to the curved surface which cannot be represented accurately by constant elements and may cause the evaluations of hypersingular integrals less accurate. For constant elements, tangential derivatives existing in the evaluation of hypersingular integrals on curved surfaces vanish. (An analytical integration approach using the HFP definition is used here for evaluating the hypersingular integrals [44]. A similar approach can be found in [45].) The fast multipole BEM, however, is found to be equally accurate as the conventional BEM, even though the number of expansion terms has changed to 10.

Figure 4 shows the CPU time used in the calculations by the conventional BEM and fast multipole BEM and with the CBIE and CHBIE. All the jobs were run on a Pentium IV 2.4 GHz laptop computer with 1 GB memory. Due to the use of a direct solver, the CBIE and CHBIE can only solve models up to a few thousands of equations (DOFs) with similar CPU time.

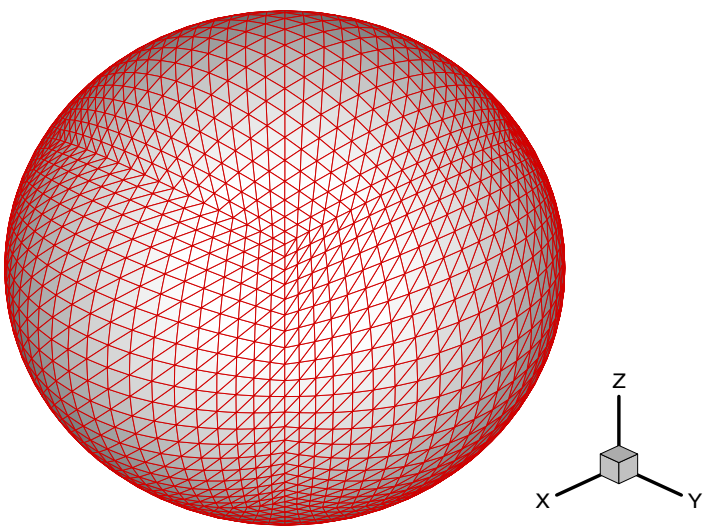

Figure 3. A spherical perfect conductor meshed with 4800 elements.

DOI: 10.1002/nme

Table II. Results for the single perfect conducting sphere.

Model	Charge density at (1, 0, 0)			
	Conventional BEM		Fast multipole BEM	
DOFs	CBIE	CHBIE	CBIE	CHBIE
768	0.987493	0.950859	0.987494	0.950862
1728	0.993770	0.966092	0.993786	0.966077
3072	0.996338	0.974311	0.996369	0.974339
4800	0.997611	0.979371	0.997817	0.979413
6912	0.998322	0.982782	0.998417	0.982684
9408	—	—	0.998979	0.985157
12 288	—	—	0.999400	0.988828
15 552	—	—	0.999697	0.990823
19 200	—	—	0.999783	0.991613
30 000	—	—	1.000990	0.994090
Exact value	1.000000			

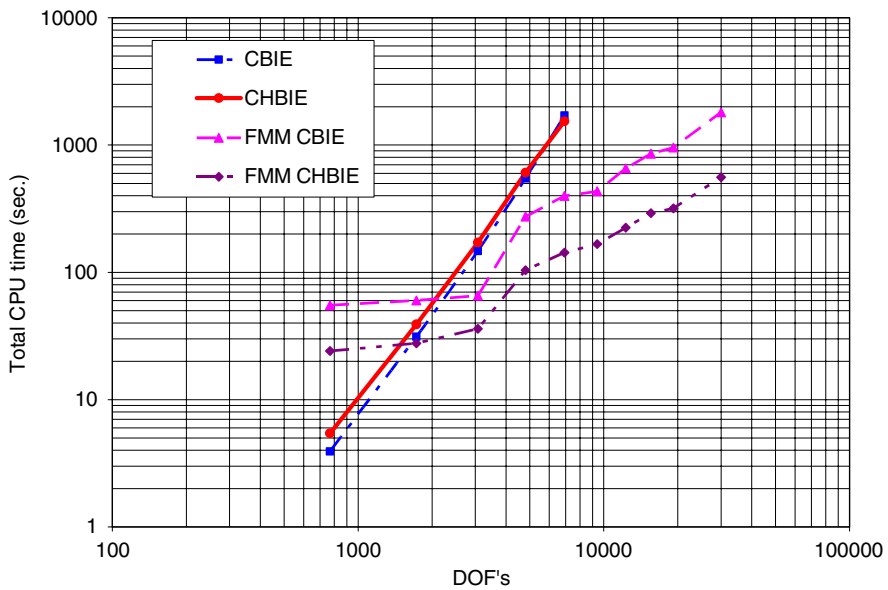

Figure 4. CPU time for the single sphere with the conventional BEM and fast multipole BEM.

The two curves have slopes close to 3 on this log–log plot, indicating an $O(N^3)$ efficiency for the conventional BEM. The two curves for the fast multipole BEM (FMM) have slopes close to 1, indicating an $O(N)$ efficiency. It is also interesting to note the significant savings with the CHBIE with the fast multipole BEM, because CHBIE has a better conditioning for the system of equations

DOI: 10.1002/nme

and thus fewer number of iterations are needed. This advantage with the CHBIE will be further demonstrated with larger models.

4.3. A multiple-conducting sphere model

In this example, 11 perfectly conducting spheres (Figure 5) are analysed with the fast multipole BEM. The centre large sphere has a radius = 3, and the 10 small spheres have the same radius = 1 and are distributed evenly on a circle with radius = 5 and co-centred with the large sphere. A constant electric potential $\phi = +5$ is applied to the large sphere and five of the small spheres and a potential $\phi = -5$ is applied to the other five small spheres (Figure 5). The potential C at the infinity is assumed to be 0. For the fast multipole BEM, elements per leaf are limited to 200, 10 terms are used in the expansions and the tolerance for convergence is set to 10^{-4}.

The charge densities on the surfaces of the spheres are plotted in Figure 6 with the mesh using 10 800 elements per sphere (again, $\varepsilon = 1$ is assumed). The plots are almost identical among the

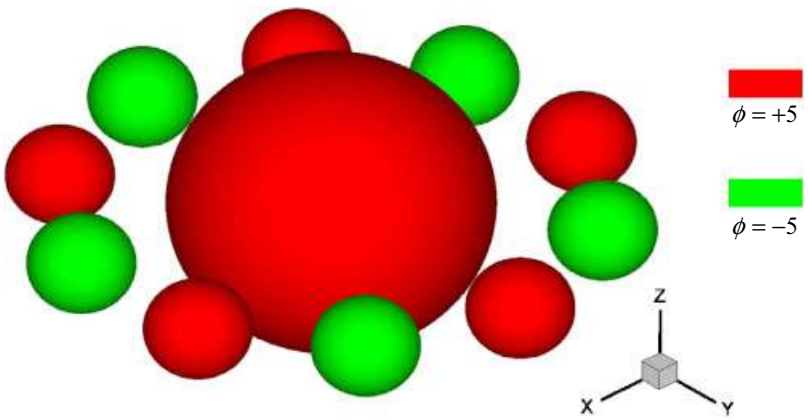

Figure 5. An 11-spherical perfect conductor model.

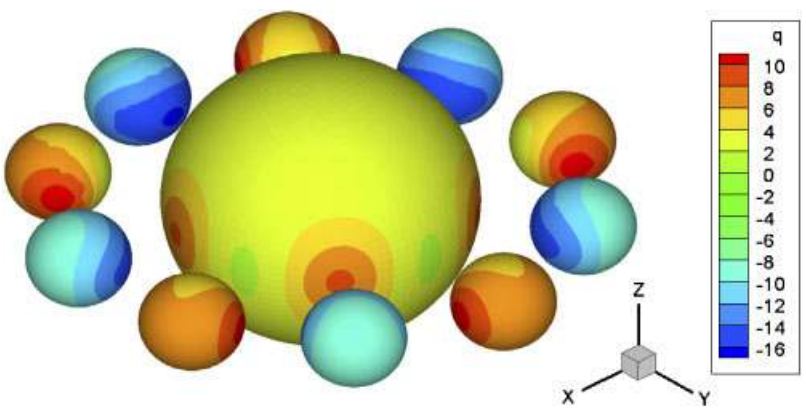

Figure 6. Contour plot of the charge densities on the spheres.

DOI: 10.1002/nme

Table III. Results for the 11-sphere model using the fast multipole BEM.

Model		Charge densities on the spheres				Numbers of iterations with the fast multipole BEM	
		Minimum		Maximum			
Elem/sphere	DOFs	CBIE	CHBIE	CBIE	CHBIE	CBIE	CHBIE
768	8448	−16.4905	−15.5285	11.1837	10.3923	14	8
1200	13 200	−16.5363	−15.7922	11.2218	10.5920	15	8
1728	19 008	−16.6322	−15.9618	11.2558	10.7156	17	8
2352	25 872	−16.6436	−16.0789	11.2746	10.8041	18	8
3072	33 792	−16.6733	−16.1618	11.3792	10.9160	19	8
3888	42 768	−16.6648	−16.2195	11.3810	10.9464	20	7
4800	52 800	−16.7435	−16.2671	11.3787	10.9763	20	8
7500	82 500	−16.7068	−16.3614	11.2964	11.0283	21	8
10 800	118 800	−17.1157	−16.4279	12.6511	11.0851	22	7

different meshes and exhibit the same symmetrical pattern as it should be. Table III shows the maximum and minimum values of the charge densities on the spheres using the different meshes. These values are very stable and converged within the first two significant digits (except for the last set of data with the CBIE). Further improvements can be achieved by using a tighter set of parameters for the fast multipole BEM (e.g. more expansion terms and smaller tolerance). The last two columns of Table III show the numbers of iterations with the GMRES solver for the CBIE and CHBIE. The numbers of iterations for the CHBIE is less than half of those for the CBIE because of the better conditioning of the systems of equations based on the CHBIE. Thus the fast multipole BEM with the CHBIE formulation can potentially converge much faster than that with the CBIE even with regularly shaped domains.

4.4. A two-parallel plate model

A two-parallel plate model (Figure 7) is considered next to verify the BIE formulations for thin shapes in the context of 3-D electrostatic analysis. A constant positive potential $\phi = 1$ is applied to the top plate, while a negative potential $\phi = -1$ applied to the bottom plate. For this problem, the analytical solution for the charge density on the lower surface of the top plate (Figure 2) is given by (see, e.g. Reference [46]):

$$\sigma = \varepsilon \frac{\partial \phi}{\partial n} = \varepsilon \frac{\Delta \phi}{\Delta n} = \frac{2\varepsilon}{g} \tag{18}$$

for the region away from the edges of the plate. This value is used to verify the BEM results. The field on the lower plate is antisymmetric with that on the top plate.

For the model studied, the parameters used are $L = 0.01$, $g = 0.001 + h$, $\varepsilon = 1$, $C = 0$ and the thickness h changes. The coupling constant in CHBIE (7) is $\beta = -(0.001 - h)$ in this case. (Again, the minus sign following the equal sign is due to the way the HBIE is added in Equation (7).) A total of 4800 elements are used on the two plates as shown in Figure 7. The number of layers of elements is reduced from five (as shown in Figure 7) to one when the thickness of the plate

DOI: 10.1002/nme

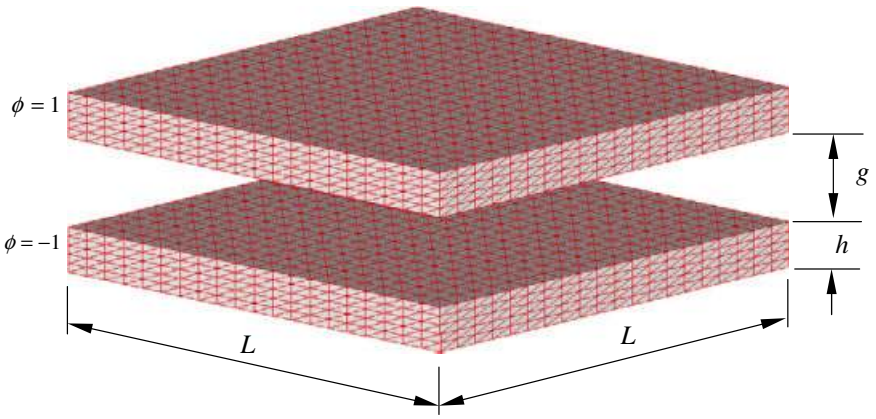

Figure 7. Two-parallel plate model (dimensions and BEM mesh).

Table IV. Charge density σ at the centre of the lower surface of the top plate in the two-plate model ($L = 0.01$, $g = 0.001 + h$, $\varepsilon = 1$, $C = 0$, 2400 elements per plate).

Model	Conventional BEM				Fast multipole BEM				Analytical solution
	CBIE		CHBIE		CBIE		CHBIE		
h/L	σ	Condition no.	σ	Condition no.	σ	No. of iterations	σ	No. of iterations	σ
1.0E − 1	1000	3.31E + 2	1000	3.31E + 2	1000	19	1000	19	1000
5.0E − 2	1333	4.60E + 2	1333	4.22E + 1	1333	18	1333	12	1333
1.0E − 2	1818	3.08E + 3	1818	4.44E + 1	1818	17	1818	12	1818
5.0E − 3	1905	6.38E + 3	1905	8.67E + 1	1905	17	1905	12	1905
1.0E − 3	1980	3.28E + 4	1980	2.96E + 2	1980	16	1980	14	1980
1.0E − 4	1998	3.75E + 5	1998	6.98E + 2	1998	16	1998	15	1998
1.0E − 5	—	8.63E + 7	2001	1.14E + 3	2000	17	2000	15	2000
1.0E − 6	—	—	2000	2.20E + 2	2000	17	2000	15	2000
1.0E − 7	—	—	1999	2.99E + 2	1998	19	2000	15	2000

Note: One layer of elements through the thickness (with 1760 elements per plate) are used for $h/L = 1.0\text{E} - 6$ and $1.0\text{E} - 7$ cases to reduce the distortion of the edge elements.

is extremely small to reduce the aspect ratios for elements on the edges. For the fast multipole BEM, 15 terms are used in the expansions and the tolerance is set to 10^{-6}.

Table IV shows the comparisons of the charge densities at the centre of the bottom surface of the top plate. The ratio h/L changes from 0.1 to 10^{-7}. The CBIE (Equation (4)) works very well until the ratio h/L reaches 10^{-4}, after which the CBIE degenerates for thin-plate problems. The CHBIE (Equation (7)) works extremely well until the ratio h/L reaches 10^{-7}. The CHBIE also shows low condition numbers with the conventional BEM and thus uses fewer iterations with the fast multipole BEM as compared with the CBIE. For the fast multipole BEM, good conditioning of a system is very important in ensuring the convergence of the solutions by iterative solvers. Thus, the CHBIE formulation, that is valid for both bulky and extremely thin structures, seems to be an ideal candidate to be used with the fast multipole BEM.

DOI: 10.1002/nme

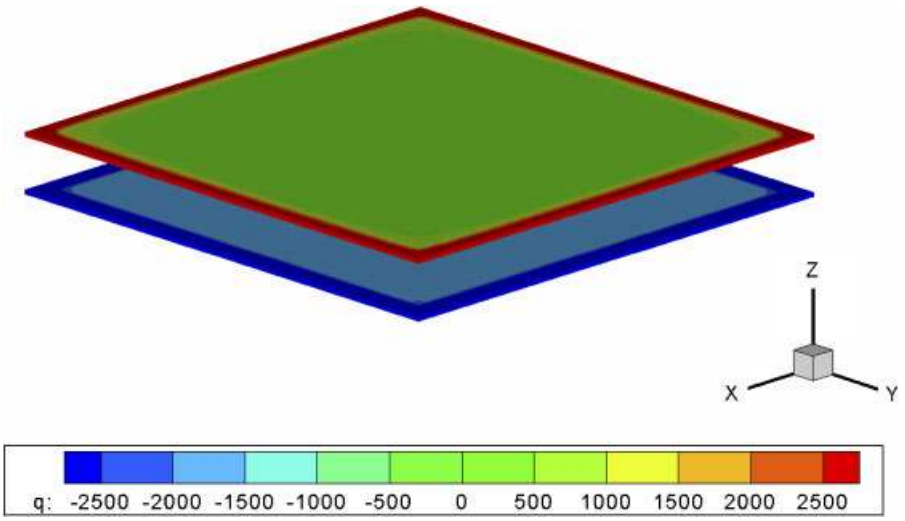

Figure 8. Charge density distribution on the parallel plates with $h/L = 0.01$.

The charge densities on the entire surfaces of the two plates are plotted in Figure 8 for the case $h/L = 0.01$. The fields in the middle of the plates are quite uniform and with opposite sign between the two plates, while the fields near the edges of the plates change rapidly. In fact, the fields near the edges and corners exhibit singularity, especially when the thickness of the plates approaches 0, thus the results near the edges require finer meshes if they are desired [9, 10, 13].

4.5. Simplified comb-drive models

Finally, simplified 3-D models of comb drives as found in MEMS are studied to demonstrate the efficiencies of the developed fast multipole BEM for solving large-scale models. Similar models have been used in [10, 13] in the 2-D cases. More realistic 3-D models of comb drives can be found in [14, 15, 24]. In the current fast multipole solutions, the numbers of expansion terms are set to 10, the maximum number of elements in a leaf to 100, and the tolerance for convergence to 10^{-4}. All the computations were done on a Dell XPS 400 desktop PC with a Pentium D 3.2 GHz CPU and 2 GB RAM. (The Fortran code is compiled with Compaq Visual Fortran V.6.6 that does not take the advantages of the dual core technology.)

The comb-drive models are built with increasing numbers of long beams applied with alternatively positive and negative electric potentials (Figure 9). The parameters used in the calculations are $L = 100$, $a = 4$, $b = 2$, $g = 3$, $d = 5$, $\varepsilon = 1$, and $C = 0$. A total of 3260 elements are used for each beam. When more beams are added into the model, the number of elements will increase accordingly so that large-scale models can be tested.

Figure 10 shows the computed charge densities with the CHBIE for a model with 55 beams. Due to the symmetry of the fields above and below each beam (except for the two outermost beams), the charge densities on the top and bottom surfaces (with the normal parallel to the z-axis) of each beam are almost symmetrical. The charge densities on any two neighbouring beams are also with the opposite sign and thus 'antisymmetric', as expected. It should be noted that the fields in

DOI: 10.1002/nme

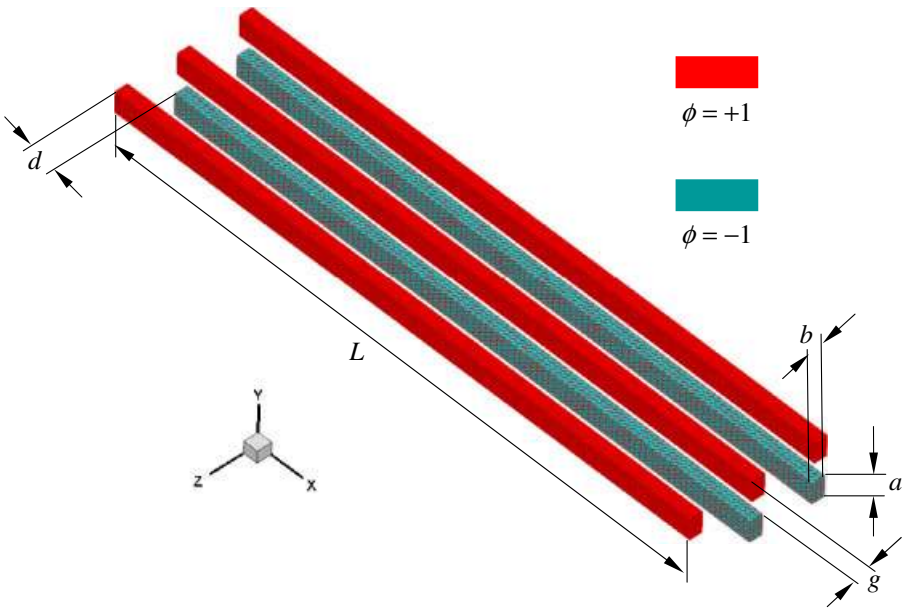

Figure 9. A simplified comb-drive model (dimensions and BEM mesh).

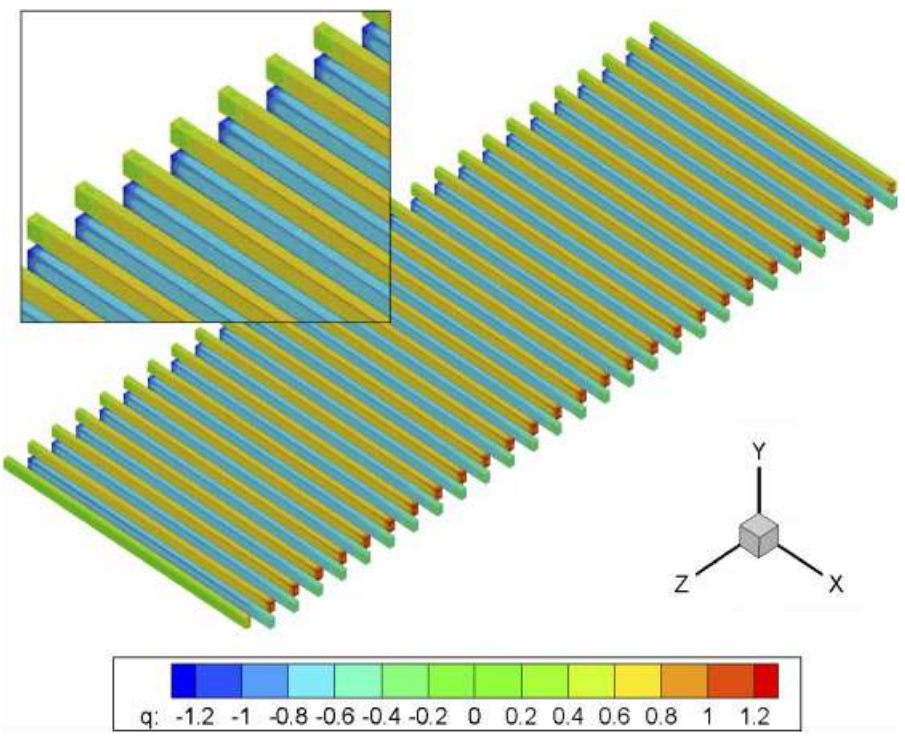

Figure 10. Charge density distribution in the comb-drive model with 55 beams.

DOI: 10.1002/nme

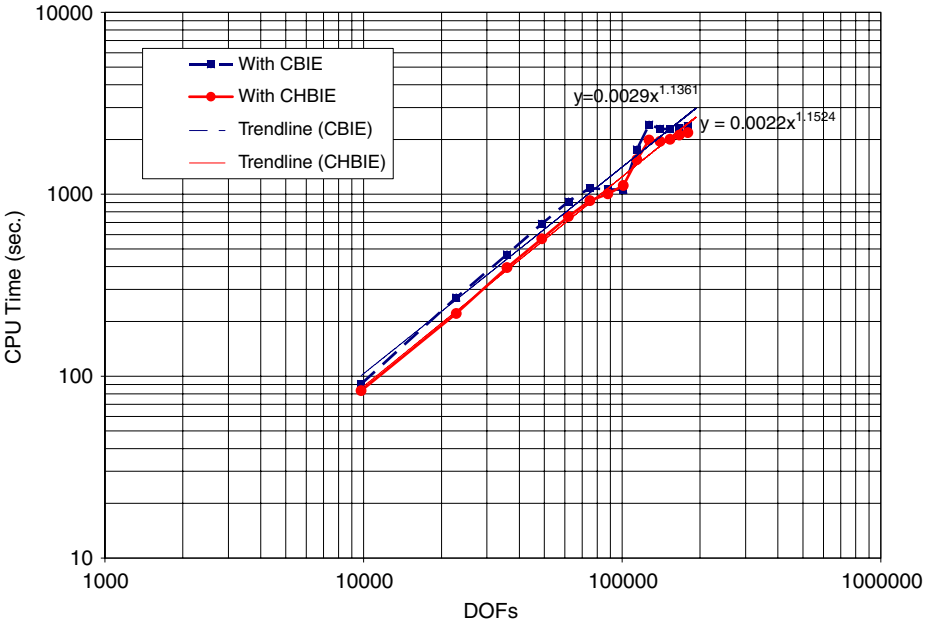

Figure 11. CPU time used for solving the comb-drive models with the fast multipole BEM (with the save option).

MEMS are much more complicated than those that the simple parallel beam models can represent, especially near the edges of the beams.

Figure 11 shows the CPU time comparison for the fast multipole BEM using the CBIE and CHBIE. As expected, the fast multipole BEM with the CHBIE converges faster than the one with the CBIE for most of the models, due to the better conditioning of the CHBIE formulation. The fast multipole BEM results converge in 17–32 iterations using the CBIE and in 13–23 iterations using the CHBIE. However, in each iteration, the CHBIE will consume more CPU time than the CBIE because of the complexity in the hypersingular kernel and its analytical integration formulas. The block diagonal preconditioner is saved in memory in these calculations so that the preconditioner and the direct evaluations of the integrals in each iteration do not need to be recalculated. With this technique, significant reduction of the CPU time can be achieved [30]. The largest model shown in Figure 11 (with 55 beams and the total DOFs = 179 300) was solved within 2200 s using the CHBIE on the Dell desktop PC. Without the save option, the same model will require about 13 000 s to solve. However, the save option will consume some amount memory of the computer and can limit the size of the problem that can be solved on the PC. Without using the save option, a large model of 445 beams with the DOFs = 1 450 700 has been solved on the same PC in about 46 h. It is estimated that this CPU time can be reduced to within 8 h if the computer has sufficiently large memory so that all the values of the preconditioner can be saved, such as on a moderate supercomputer with 20 GB RAM. (See [47, 48] for the performance of the fast multipole BEM on supercomputers for modelling large-scale 3-D problems.)

This example clearly demonstrates the efficiency and potential of the developed 3-D fast multipole BEM based on the CHBIE formulation for large-scale electrostatic analysis.

DOI: 10.1002/nme

5. DISCUSSIONS

A dual BIE (CHBIE) formulation for modelling 3-D electrostatic problems is investigated in this study. It is found that the dual BIE yields relatively small condition numbers for regions containing either bulky or thin structures and thus is better suited for implementation with the fast multipole BEM. The new adaptive fast multipole BEM is implemented for the CHBIE formulations based on the fast multipole BEM code developed in Reference [30] using the CBIE only. Several example problems are studied using the developed fast multipole BEM code to test the accuracy and efficiency. The results of these examples clearly demonstrate that the CHBIE is very effective in solving problems with either bulky or thin structures and the fast multipole BEM based on the CHBIE is very promising in solving large-scale models.

The developed code is for general potential problems using the dual BIE approach, that involves four integrals. The efficiency of the code can be improved significantly if one is only interested in studying perfect conductor cases, where the F integral in CBIE (4) and H integral in HBIE (5) can be dropped due to the properties of the kernels (see, e.g. References [13, 34]), as in the 2-D cases [13]. Higher-order elements may also be employed with the fast multipole BEM in order to improve the accuracy of the code and possibly the efficiency as well. For flat structures, such as the MEMS models, the binary tree approach [25] may be more efficient.

Using the developed code, more complicated and realistic MEMS models can be studied and more interesting physics can be investigated. The electric forces on the conducting structures can be obtained readily from the calculated charge densities. Structural deformation can then be studied using a fast multipole BEM code for elasticity problems. Furthermore, fast multipole BEM codes for coupled electro-mechanical, dynamic, and non-linear problems can be developed.

ACKNOWLEDGEMENTS

This research has been supported by grant CMS-0508232 of the U.S. National Science Foundation. The authors would also like to thank Professor Subrata Mukherjee at Cornell University for many helpful discussions on modelling MEMS problems with the BEM and for his constructive comments on this paper.

REFERENCES

1. Mukherjee S. *Boundary Element Methods in Creep and Fracture*. Applied Science Publishers: New York, 1982.
2. Cruse TA. *Boundary Element Analysis in Computational Fracture Mechanics*. Kluwer Academic Publishers: Dordrecht, The Netherlands, 1988.
3. Brebbia CA, Dominguez J. *Boundary Elements—An Introductory Course*. McGraw-Hill: New York, 1989.
4. Banerjee PK. *The Boundary Element Methods in Engineering* (2nd edn). McGraw-Hill: New York, 1994.
5. Kane JH. *Boundary Element Analysis in Engineering Continuum Mechanics*. Prentice-Hall: Englewood Cliffs, NJ, 1994.
6. Shi F, Ramesh P, Mukherjee S. Simulation methods for micro-electro-mechanical structures (MEMS) with application to a microtweezer. *Computers and Structures* 1995; **56**:769–783.
7. Ye W, Mukherjee S. Optimal shape design of three-dimensional MEMS with applications to electrostatic comb drives. *International Journal for Numerical Methods in Engineering* 1999; **45**:175–194.
8. Ye W, Mukherjee S. Design and fabrication of an electrostatic variable gap comb drive in micro-electro-mechanical systems. *Computer Modeling in Engineering and Sciences* 2000; **1**:111–120.
9. Bao Z, Mukherjee S. Electrostatic BEM for MEMS with thin conducting plates and shells. *Engineering Analysis with Boundary Elements* 2004; **28**:1427–1435.

DOI: 10.1002/nme

10. Bao Z, Mukherjee S. Electrostatic BEM for MEMS with thin beams. *Communications in Numerical Methods in Engineering* 2005; **21**:297–312.
11. De SK, Aluru NR. Full-Lagrangian schemes for dynamic analysis of electrostatic MEMS. *Journal of Microelectromechanical Systems* 2004; **13**:737.
12. Chyuan S-W, Liao Y-S, Chen J-T. Computational study of the effect of finger width and aspect ratios for the electrostatic levitating force of MEMS combdrive. *Journal of Microelectromechanical Systems* 2005; **14**:305–312.
13. Liu YJ. Dual BIE approaches for modeling electrostatic MEMS problems with thin beams and accelerated by the fast multipole method. *Engineering Analysis with Boundary Elements* 2006; **30**:940–948.
14. Frangi A. A fast multipole implementation of the qualocation mixed-velocity-traction approach for exterior Stokes flows. *Engineering Analysis with Boundary Elements* 2005; **29**:1039–1046.
15. Frangi A, Tausch J. A qualocation enhanced approach for Stokes flow problems with rigid-body boundary conditions. *Engineering Analysis with Boundary Elements* 2005; **29**:886.
16. Mukherjee S, Telukunta S, Mukherjee YX. BEM modeling of damping forces on MEMS with thin plates. *Engineering Analysis with Boundary Elements* 2005; **29**:1000–1007.
17. Rokhlin V. Rapid solution of integral equations of classical potential theory. *Journal of Computational Physics* 1985; **60**:187–207.
18. Greengard LF, Rokhlin V. A fast algorithm for particle simulations. *Journal of Computational Physics* 1987; **73**:325–348.
19. Greengard LF. *The Rapid Evaluation of Potential Fields in Particle Systems*. The MIT Press: Cambridge, 1988.
20. Nishimura N. Fast multipole accelerated boundary integral equation methods. *Applied Mechanics Reviews* 2002; **55**:299–324.
21. Liu YJ, Nishimura N. The fast multipole boundary element method for potential problems: a tutorial. *Engineering Analysis with Boundary Elements* 2006; **30**:371–381.
22. Nabors K, White J. FastCap: a multipole accelerated 3-D capacitance extraction program. *IEEE Transactions on Computer-Aided Design* 1991; **10**:1447–1459.
23. Ljung P, Bachtold M, Spasojevic M. Analysis of realistic large MEMS devices. *Computer Modeling in Engineering and Sciences* 2000; **1**:21–30.
24. Frangi A, Gioia Ad. Multipole BEM for the evaluation of damping forces on MEMS. *Computational Mechanics* 2005; **37**:24–31.
25. Urago M, Koyama T, Takahashi K, Saito S, Mochimaru Y. Fast multipole boundary element method using the binary tree structure with tight bounds: application to a calculation of an electrostatic force for the manipulation of a metal micro particle. *Engineering Analysis with Boundary Elements* 2003; **27**:835–844.
26. Masters N, Ye W. Fast BEM solution for coupled 3D electrostatic and linear elastic problems. *Engineering Analysis with Boundary Elements* 2004; **28**:1175–1186.
27. Ding J, Ye W. A fast integral approach for drag force calculation due to oscillatory slip Stokes flows. *International Journal for Numerical Methods in Engineering* 2004; **60**:1535–1567.
28. Krishnasamy G, Rizzo FJ, Liu YJ. Boundary integral equations for thin bodies. *International Journal for Numerical Methods in Engineering* 1994; **37**:107–121.
29. Liu YJ, Rizzo FJ. Scattering of elastic waves from thin shapes in three dimensions using the composite boundary integral equation formulation. *Journal of the Acoustical Society of America* 1997; **102**(2):926–932.
30. Shen L, Liu YJ. An adaptive fast multipole boundary element method for three-dimensional potential problems. *Computational Mechanics*, in press (Published online 15 March 2006).
31. Krishnasamy G, Rizzo FJ, Rudolphi TJ. Hypersingular boundary integral equations: their occurrence, interpretation, regularization and computation. In *Developments in Boundary Element Methods* (Chapter 7), Banerjee PK *et al*. (eds). Elsevier Applied Science Publishers: London, 1991.
32. Sladek V, Sladek J (eds). In *Singular Integrals in Boundary Element Methods*, *Advances in Boundary Element Series*, Brebbia CA, Aliabadi MH (eds). Computational Mechanics Publications: Boston, 1998.
33. Mukherjee S. CPV and HFP integrals and their applications in the boundary element method. *International Journal of Solids and Structures* 2000; **37**:6623–6634.
34. Liu YJ, Rudolphi TJ. Some identities for fundamental solutions and their applications to weakly-singular boundary element formulations. *Engineering Analysis with Boundary Elements* 1991; **8**:301–311.
35. Perez-Gavilan JJ, Aliabadi MH. A symmetric Galerkin BEM for multi-connected bodies: a new approach. *Engineering Analysis with Boundary Elements* 2001; **25**:633–638.
36. Perez-Gavilan JJ, Aliabadi MH. Symmetric Galerkin BEM for multi-connected bodies. *Communications in Numerical Methods in Engineering* 2001; **17**:761–770.

DOI: 10.1002/nme

37. Frangi A, Novati G. Symmetric BE method in two-dimensional elasticity: evaluation of double integrals for curved elements. *Computational Mechanics* 1996; **19**:58–68.
38. Liu YJ. Analysis of shell-like structures by the boundary element method based on 3-D elasticity: formulation and verification. *International Journal for Numerical Methods in Engineering* 1998; **41**:541–558.
39. Mukherjee S. On boundary integral equations for cracked and for thin bodies. *Mathematics and Mechanics of Solids* 2001; **6**:47–64.
40. Burton AJ, Miller GF. The application of integral equation methods to the numerical solution of some exterior boundary-value problems. *Proceedings of the Royal Society of London*, *Series A* 1971; **323**:201–210.
41. Liu YJ, Rizzo FJ. A weakly-singular form of the hypersingular boundary integral equation applied to 3-D acoustic wave problems. *Computer Methods in Applied Mechanics and Engineering* 1992; **96**:271–287.
42. Yoshida K. Applications of fast multipole method to boundary integral equation method. *Ph.D. Dissertation*, Department of Global Environment Engineering, Kyoto University, 2001.
43. Yoshida K, Nishimura N, Kobayashi S. Application of new fast multipole boundary integral equation method to crack problems in 3D. *Engineering Analysis with Boundary Elements* 2001; **25**:239–247.
44. Fukui T. Research on the boundary element method—development and applications of fast and accurate computations. *Ph.D. Dissertation*, Department of Global Environment Engineering, Kyoto University, 1998 (in Japanese).
45. Mukherjee S. Finite parts of singular and hypersingular integrals with irregular boundary source points. *Engineering Analysis with Boundary Elements* 2000; **24**:767–776.
46. Hayt WH, Buck JA. *Engineering Electromagnetics*. McGraw-Hill: London, 2001.
47. Liu YJ, Nishimura N, Otani Y, Takahashi T, Chen XL, Munakata H. A fast boundary element method for the analysis of fiber-reinforced composites based on a rigid-inclusion model. *Journal of Applied Mechanics* 2005; **72**:115–128.
48. Liu YJ, Nishimura N, Otani Y. Large-scale modeling of carbon-nanotube composites by the boundary element method based on a rigid-inclusion model. *Computational Materials Science* 2005; **34**:173–187.

DOI: 10.1002/nme